Exploring the properties of Dy_2O_3–Y_2O_3 Co-activated telluro-borate glass: Structural, physical, optical, thermal, and mechanical properties

Hammam Abdurabu Thabit [a,*], Abd Khamim Ismail [a], M.H.A. Mhareb [b,c], D.A. Abdulmalik [d], Abdullahi I [a,e], Abdo Mohammed Al-Fakih [f], Y.S.M. Alajerami [g], S.Hashim [a]

[a] *Department of Physics, Universiti Teknologi Malaysia, 81310, Johor Bahru, Malaysia*
[b] *Department of Physics, College of Science, Imam Abdulrahman Bin Faisal University, P.O. Box 1982, Dammam 31441, Saudi Arabia*
[c] *Basic and Applied Scientific Research Center, Imam Abdulrahman Bin Faisal University, PO Box 1982, Dammam 31441, Saudi Arabia*
[d] *Department of Mathematics, Statistics and Physics, College of Arts and Sciences, Qatar University, 2713, Doha, Qatar*
[e] *Physics Department, Federal University Gusau Zamfara State Nigeria*
[f] *Department of Chemistry, Faculty of Science, Universiti Teknologi Malaysia, Johor, Malaysia*
[g] *Department of Medical Radiography, Al-Azhar University, Gaza Strip, Palestine*

ARTICLE INFO

ABSTRACT

The successful application of glass-based materials in a wide range of scientific fields depends on the associated physical, optical, thermal, and mechanical properties. This article investigate the structural, Physical, thermal, optical, and mechanical properties of Dy_2O_3, Y_2O_3 co-activated telluro-borate glass developed using the melt-quenching method. The glassy quality and the elements component of the specimens were observed using XRD and EDX analyses. The addition of Y_2O_3 rise the glass density from 2.956 to 3.303 g/cm^3 the refractive index from 2.5 to 2.7. These changes are due to the increase in polarizability and non-bridging oxygen (NBO). The photoluminescence (PL) spectra revealed a broad peak at 550 nm and additional weak emission peaks at 573 and 664 nm, respectively. While the observed broader peak can be linked to the convolution of Bi^{3+} ions transitions corresponding to the non-centrosymmetric site respectively, the weak emission bands are due to $^4F_{9/2} \rightarrow {}^6H_{13/2}$ and $^4F_{9/2} \rightarrow {}^6H_{11/2}$ Dy^{3+} transitions. Hence, the low symmetrical features of both Bi^{3+} and Dy^{3+} ions were confirmed. The increase in the Vickers hardness of the glass from 536.7 to 1366.9 indicates the influence of Y_2O_3 addition on the mechanical properties of the glasses. The findings help to improve our understanding of the behaviour of the glass composition and its prospective applications in disciplines such as photonic, and laser optics.

1. Introduction

Over the last few years, solid-state sources have become more technologically important in lighting and displays. The development of photonic devices such as inorganic, organic light-emitting diodes (LEDs) and lasers allows for a new era of technological

---

advancement. Optoelectronic devices greatly influence the fabrication and manufacturing of substances for innovative electronic appliances [1]. The glasses doped with rare earth also provide well-characterized glow colors [2–7]. In addition to discerning their implementations in solid-state lighting tools, the analysis of photoluminescence for materials doped with rare-earth can assist in realizing their use in optoelectronic tools, for instance, frequency up/down converters in solar cells and lasers [8,9]. Transition metals (TM) and rare earth elements have been combined with activated glass hosts to generate lasers and other optoelectronic devices efficiently [10]. The above applications require improving new inorganic glass systems doped with rare earth [11,12].

Rare earth elements have luminescent properties that rely on their impurity ions and host composition. Dysprosium (Dy^{3+}) is an exciting center for scientists as it can produce robust fluorescence in visible blue-yellow regions. Thus, Dy^{3+} ion-activated glassy substances have explored for possible uses for luminescence, plasma displays, CRT tubes, visible lasers, high-density optical memories, solid-state devices, undersea communication, radiation dosimeters, etc. [13–16]. Dy^{3+} ions have two emission peaks emitting from the green to the blue region, which happen from the ${}^4F_{9/2}$-${}^6H_{13/2}$ and ${}^4F_{9/2}$-${}^6H_{15/2}$ transitions for yellow and blue respectively [13,17–19]. Various oxides have been used as hosts for rare earth ion dopants, such as phosphates, silicates, fluorides, tellurite, and borates. Borate-based glasses have special physical and optical properties that differentiate them from other glasses. These properties include simplicity of production, low melting point, affordability, outstanding heat stability, high optical transparency, and exceptional glass-forming capacity [20]. Numerous successful industrial applications, such as sodium vapor lamps, solder glasses (low-temperature sealing glasses), solid-state lasers, bioactive glasses, radiation dosimetry, and gamma-ray shielding, have been drawn by unique properties [21–26]. However, borate-based glasses have certain complex limitations, including poor chemical durability, extreme hygroscopicity, and high phonon energies (1400 cm^{-1}), that increase the non-radiative emission losses and reduce the radiative transition rate. Because borate glasses are not appropriate as efficient laser host materials to minimize radiative losses in borate systems, tellurium oxide (TeO_2) is ideal for borate additions because the pre-host suppresses excess phonon energy and increases radiative transition rates [27]. Introducing a second component, such as tellurite, to borate-based glass matrices can reduce the hygroscopic features, which proved to be an efficient way of mitigating the problems mentioned above. Thus, for optimum performance, these drawbacks need to be addressed. Tellurite glasses have many desirable properties, including high dielectric constant, good corrosion resistance, low melting point (733 °C), low phonon energy (approximately 700 cm^{-1}), high refractive index, good thermal and chemical stability, good ionic conductivity, as well as a wide transmission range in the visible and near infra-red (360–6500 nm) region [28]. Many studies have shown that adding tellurite as a second component to the matrix may enhance borate-based glasses' physical and optical properties [29,30]. Tellurite in the borate matrix disrupts the typical B–O bonding by only slackly connecting with the oxygen atoms. More tetrahedral boron units are formed by breaking the bridging oxygen link and forming the non-bridging oxygen bond (by replacing the B–O bond with the Te–O bond). Adding heavy metals such as Bi_2O_3 to B_2O_3 can enhance radiative emissivity [31,32]. Heavy metal oxide (Bi_2O_3) glasses are known for their optical properties, refractive index, high polarizability, high-valent cations, low chemical durability, and low field strength [31]. Based on previous findings, alkaline metals like barium, magnesium, calcium, strontium, etc., can enhance the optical basicity and change the energy states of the glass host. Adding SrO as network modifiers avoided devitrification for the glass host [33]. Furthermore, the SrO has low field strength that nominates it to be an excellent modifier that alters the local symmetry surrounding the borate, decreasing the thermal expansion coefficient and improving glass-forming stability. Adding SrO can transform BO_3 into BO_4, decreasing the non-bridging oxygen (NBOs). In addition, SrO inside the glass host improves the glass structure and reduces moisture and stiffness of the glass network due to the higher field strength surrounding the borates. Moreover, SrO is a fluxing substance, resulting in the produced glass's strength and durability. Besides, it possesses a moderate level of surface tension and viscosity, along with a high rate of contraction and expansion [34,35]. This article aims to study the influence of addition Dy^{3+} ions and co-activated Y_2O_3 on the physical, optical, photoluminescence, mechanical, structural, and thermal features of the B_2O_3–TeO_2–SrO–Bi_2O_3–ZnO glass system.

2. Experimental

2.1. Glass synthesis

A series of glasses (70)B_2O_3-(7.8)TeO_2-(20)SrO-(1)Bi_2O_3-(1)ZnO-(0.2)Dy_2O_3–(0)Y_2O_3, and (70)B_2O_3-(7.8)TeO_2-(15)SrO-(1)Bi_2O_3-(1)ZnO-(0.2)Dy_2O_3–(5)Y_2O_3 was fabricated by using the melt-quenching approach method. All chemical compositions made by Sigma Aldrich (99.999%) and available in materials science lab C21, faculty of Science (FS) Universiti Teknologi Malaysia UTM. Table 1 shows the BTSY0 and BTSY1 glasses produced using chemical raw materials, including B_2O_3, TeO_2, SrO, ZnO, Bi_2O_3, Dy_2O_3, and Y_2O_3 in powder form. The powders were accurately weighed and mixed thoroughly using mortar to ensure a symmetrical powder. The

Table 1
Physical and optical properties of the prepared glass samples.

Physical/optical parameters	BTSY0	BTSY1
Y_2O_3 mol%	0	5
Density (g/cm^3) ± 0.12	2.956	3.30
Molar volume (cm^3/mol) ± 0.7	29.811	28.52
Mol.w. (g/mol)	94.233	88.12
Band gap energy E_g (eV)	2.550	1.710
refraction index n	2.500	2.87

resulting mixture was melted in an aluminum crucible for 45 min at 1000 °C. During the melting time, the sample was taken out and agitate the liquid solution quickly to eliminate air bubbles and achieve homogeneity. To reduce thermal stress and strain, the molten glass was poured onto a plate of stainless steel within an annealing furnace and heated to 400 °C for 6 h. The glasses' molar volume and density were quantified using toluene via the Archimedes technique. The physical properties were determined and listed in Table 1. The index of refraction (n = c/v), which plays a crucial role in the interaction between electromagnetic waves and the dielectric medium, was also calculated using the band gap obtained from the procedure described below.

The density (ρ) measurement was carried out by employing Archimedes' principle and Equation (1) [1].

$$\rho = \frac{W_a}{W_a - W_b} \times \rho_T \tag{1}$$

W_a refers to the weights of the glass in air, W_b, the weights of the glass in toluene medium, and ρ_T is the density of toluene.

Equation (2) is used to get the molar volume (V_m) of each glass, which is calculated by dividing the molar weights (M) by the density (ρ) Equation (2) [36]:

$$V_m = \frac{M_w}{\rho} \tag{2}$$

The following equation (3) is used to extrapolate the linear part curve of $(h\nu)^2$ vs the photon energy ($h\nu$) in order to get the band gap [37]:

$$\alpha h v = \left(hv - E_g\right)^m \tag{3}$$

Where hv is the photon energy, α is the absorption coefficient calculated from the absorption data, and m = 1/2 for the direct transition bandgap. E_g is the direct optical band gap energy.

The refractive index (n) was estimated via following Equation (4) [6], wherein E_g is the band gap.

$$n^2 + 2 = \sqrt{180/E_g} \tag{4}$$

2.2. Glass characterization

Various methods were employed to determine the physical and chemical characteristics of the glass samples. The glass structural was determined using XRD analysis conducted with a Pan-alytical diffractometer (PW, 3040 MPD). Vibrational modes of the glass systems were evaluated under 532 nm excitation, using wavenumbers ranging from 250 to 1750 cm^{-1}, using a Bruker FT-Raman, Multi-RAM spectrometer. The elemental composition of the glasses was determined through examination with an energy-dispersive X-ray spectroscopy (EDX). Additionally, the photoluminescence spectra (PL) under 350 nm excitation were measured using a Perki-nElmer LS55 Luminescence Spectrophotometer, at room temperature. Finally, the thermal analysis of the glasses specimens were conducted via PerkinElmer differential thermal analysis/thermogravimetry analysis (DTA/TGA).
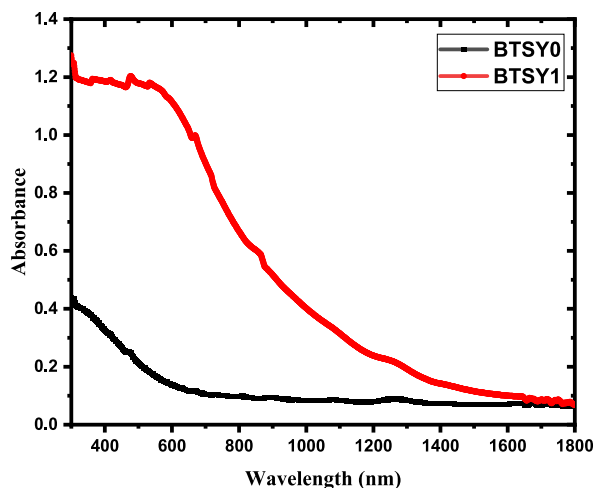

Fig. 1. Absorption spectra for telluro-borate glass system/doped BTSY0 and co-doped BTSY1.

3. Results

3.1. The physical and optical glassy characteristics

Table 1 shows some optical and physical parameters. The density is the main parameter because it can be used to calculate other parameters. Adding Y2O3 instead of SrO enhanced the density from 2.956 to 3.303 g/cm3; this enhancement in density values results from replacing a molecule with a low molar mass (SrO) with another with a higher molar mass (Y_2O_3). Conversely, the molar volume significantly reduced from 32.514 to 26.864 cm^3/mol. The inverse relationship between density and molar volume indicates the increase in the compactness of the BTSY1 sample compared with the BTSY0 sample. Fig. 1 displays the UV–Vis–NIR absorption spectrum for BTSY0 and BTSY1 glasses. From the UV absorption edge, the band gap for BTSY0 and BTSY1 glasses was determined and drawn in Fig. 2. Table 1 enlists the band gap and refractive index values. The addition of Y_2O_3 reduced the band gap from 2.55 to 1.71 eV, indicating the enhancement of the localization degree due to defects forming the formation defects in the charge distribution. So, the oxygen energy levels are close to the valence band, leading to a rise in the donor centers' number in the glass network; therefore, the band gap decreases [10,38]. At the same time, the refractive index results increased from 2.5 to 2.7 due to increased non-bridging oxygen (NBO) and polarizability.

3.2. Structural and morphological properties

Fig. 3 illustrates the XRD pattern of the fabricated BTSY0 and BTSY1 glasses. This figure shows the broad peaks 28 and 48°, affirming the absence long-order range that indicates the amorphous nature of BTSY0 and BTSY1 glasses.

The Raman spectrum for BTSY0 and BTSY1 glasses is displayed in Fig. 4. This spectrum shows three peaks centered at 443–470, 777, and 1445 cm^{-1}. The peaks centered at 443-470 cm^{-1} are assigned to stretching vibrations of Te–O–Te bonds. This peak showed a shift from 470 to 443 cm^{-1} with adding Y_2O_3 instead of SrO, indicating a reduction of the contribution of Te–O–Te bonds and the formation of new bonds Y–O–Te. These bonds can enhance the glass's stability. Another peak is at 777 cm^{-1}, ascribed to stretching vibrations of TeO$_3$/TeO$_{3+1}$. This peak became broad with adding Y_2O_3 instead of SrO at a lower wavenumber, which is attributed to reducing the TeO$_3$/TeO$_{3+1}$ and starting to shift to TeO$_4$, which enhances glass stability. The last peak at 1445 cm^{-1} relates to B–O stretching in metaborate rings and chain units [39].

The EDX results for BTSY0 and BTSY1 glass samples are shown in Fig. 5a and b. It can be noted that there is no contamination in the two glass samples. In addition, the EDX shows the existence of Y in the BTSY1 glass sample, which was added instead of Sr, as illustrated in Fig. 5b. Table 2 includes the atomic and weight data for several elements obtained from the EDX studies. However, the EDX spectra's intensity for each peak for each element varied from composition to composition, indicating that the intensity of each element is influenced by its concentration [40].

3.3. Thermal properties

Investigating glasses' phase transformations and thermal stability is essential to understand their potential applications and transport behaviors. A glass system's working temperature can be determined by the transition temperature (T_g). The known T_g indicates the maximum working temperature for this glass and provides a good knowledge of the glass network bond and connectivity.
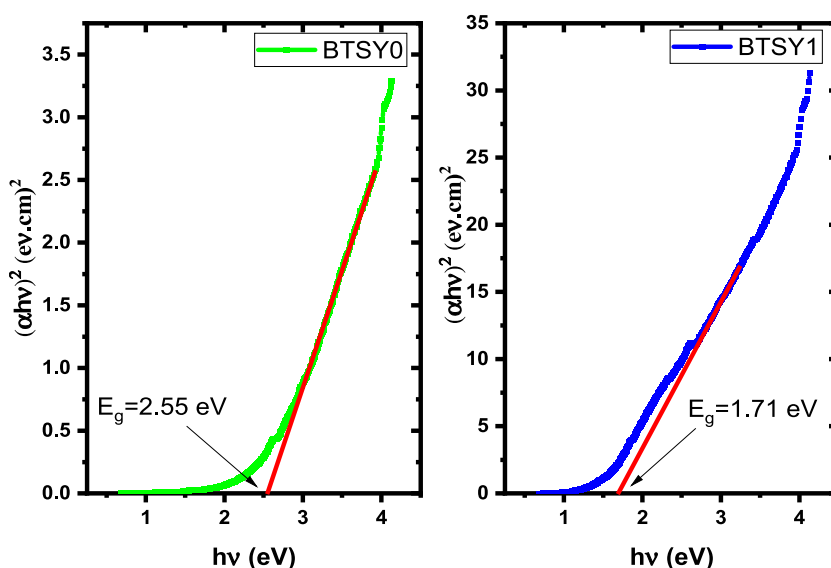

Fig. 2. Bandgap for telluro-borate glass system/doped BTSY0 and co-doped BTSY1.
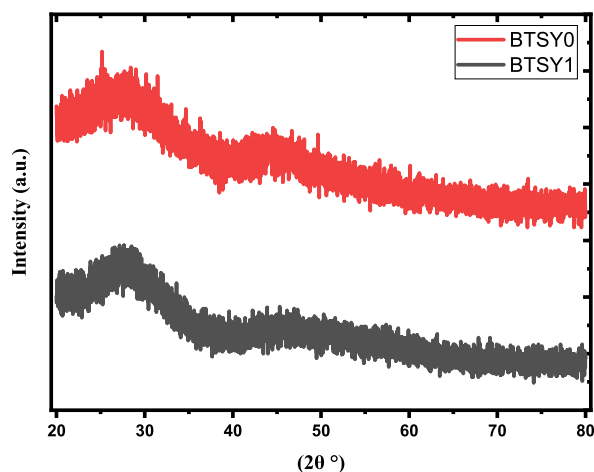
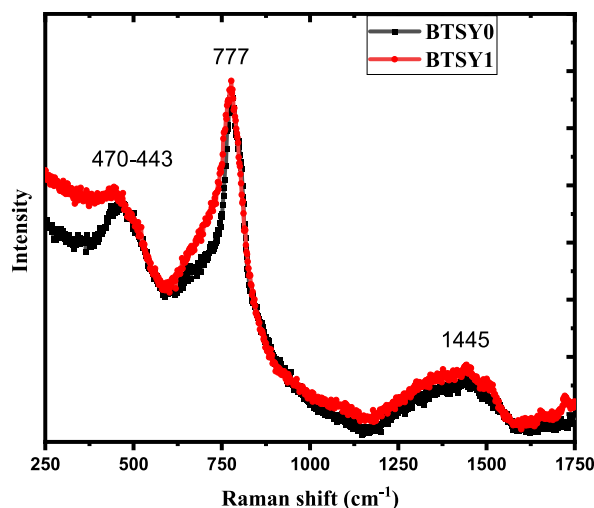**Fig. 3.** XRD pattern of BTSY0 and BTSY1 glasses.

Fig. 4. Raman spectrum for telluro-borate glass system/doped BTSY0 and co-doped BTSY1.

Generally, the glass with high cross-linking and connection has high T_g values [41]. Conversely, loosely packed glass has a low T_g [41]. Fig. 6a shows the differential thermal analysis/thermogravimetric analysis (DTA/TGA) for BTSY0 and BTSY1. Table 2 illustrates some of the calculated values based on the extracted values from Fig. 6a and b. From Table 3, the T_g values increase with the addition of Y_2O_3. The direct relation between the increasing T_g and density values affirms the previous arguments and our argument strengthens the inverse relationship between T_g and molar volume.

The glass with high density and low molar volume has high compactness and packing density. The $\Delta T = T_c\text{-}T_g$ is a parameter used to measure the thermal stability against crystallization for any glass system. The high ΔT values indicate higher glass resistance for crystallization. So, the BTSY0 sample showed an optimum value compared with BTSY1. The $(T_c\text{-}T_g)/T_c$ parameter supports the ΔT result, indicating high stability against crystallinity for the BTSY0 sample [42]. Another parameter, T_g/T_m, is called reduced glass transition temperature [43]. This parameter can be used to evaluate the ability to convert to crystal if the T_g/T_m is more significant than 0.60, indicating difficulty converting to crystal. In this case, the glass surface will become only crystal when exposed to heat treatment. The T_g/T_m values for BTSY0 and BTSY1 are 0.63 and 0.64. The TGA spectrum for BTSY0 and BTSY1 recorded weight loss of 2.850 and 2.593% at 1000 °C, respectively, [44]. Adding Y_2O_3 reduced the weight loss of BTSY0 glass, affirming the enhancement of glass stability. The obtained results are in line with T_g values for BTSY0 and BTSY1.

3.4. The relation between thermal and physical properties

The relation between different physical properties and T_g values was studied. The packing density is a parameter that can determine the glass structure changes. From Tables 3 and 4, it can be noted that there is a relation between the physical properties and T_g values.
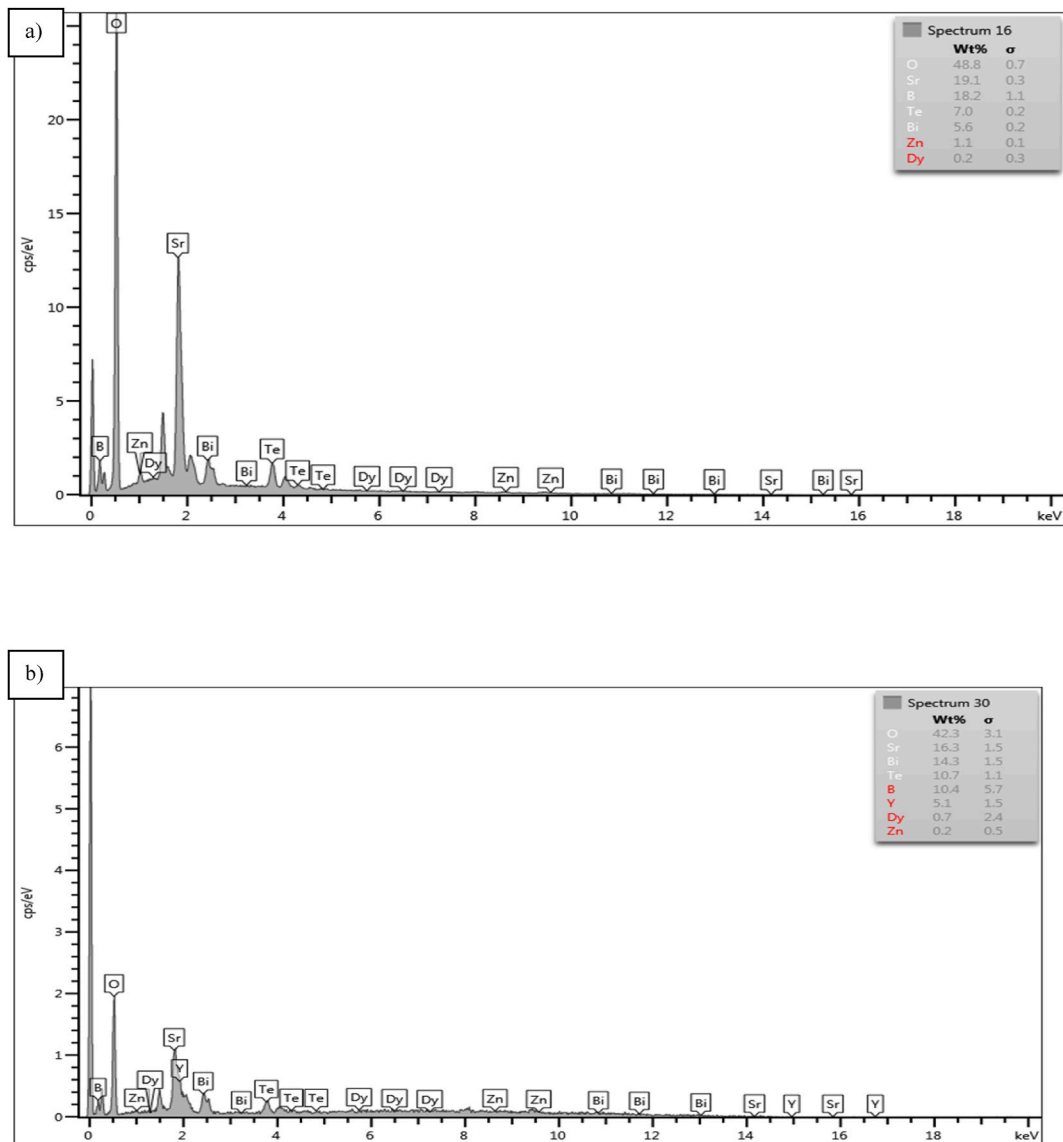
Fig. 5. EDX spectrum of BTSY0 and co-doped BTSY1.

The V_t values increased from 0.627 to 0.676 with increasing Y_2O_3; this increment in V_t affirms the increment in T_g results. So, the BTSY1 glass sample with the highest V_t and T_g is more closely packed and thermally stable than the BTSY0 sample. The main atomic volume ($\overline{V}$) can be used to understand the variation in T_g values. The inverse relation between main atomic volume and glass rigidity was suggested by Bhatti and Singh [45]. From Table 4, the values of $\overline{V}$ reduced from 7.07 to 6.54 cm^3/mol with adding Y_2O_3. This result is in line with Bhatti and Singh's relation. Zaho et al., [46] assumed a relation between T_g and $\overline{V}$ for metallic glasses, and they found the following Equation (5), [46]:

$$T_g = \frac{C}{\overline{V}^\beta}$$

(5)

Here, the C and β are constants. The inverse relation between the T_g and $\overline{V}$ Values affirm the Zaho relation. Abd El-Moneim and Alfifi's approach [47] suggested another parameter to estimate glass rigidity: the ratio of packing density to mean atomic volume ($V_t/\overline{V}$). Therefore, a high ($V_t/\overline{V}$) ratio indicates that the glass is more rigid. As seen in Table 4, the ($V_t/\overline{V}$) ratio increased from 0.088 to 0.103, which fully agreed with the T_g results.

The single bond strength (B_{A-O}) for the participating element in the glass system network can be used to explain the change in T_g values. According to the electronegativity of each component, as shown in Table 4, the nature of bonds for Bi–O, B–O, and Ti–O is covalent, while the bonds nature for Sr–O, Zn–O, Dy–O, and Y–O are ionic. According to Sun [48], the B_{A-O} of A-O in any oxide can be

Table 2
Elemental compositions in glasses BTSY0 and BTSY1 were obtained from EDX analyses.

Element Of BTSY0	Line Type	Apparent Concentration	Intensity Correction	k Ratio	Wt%	Wt% Sigma	Atomic %
B	K series	0.00	0.33	0.00000	0.00	0.00	0.00
O	K series	14.49	0.96	0.04875	60.54	0.46	90.85
Zn	L series	0.12	0.37	0.00124	1.36	0.18	0.50
Sr	L series	4.69	0.82	0.04130	22.94	0.30	6.28
Te	L series	1.89	0.89	0.01460	8.49	0.24	1.60
Dy	L series	0.04	0.68	0.00038	0.22	0.39	0.03
Bi	M series	0.99	0.62	0.00993	6.45	0.34	0.74
Total:					100.00		100.00
Element Of BTSY1	Line Type	Apparent Concentration	Intensity Correction	k Ratio	Wt%	Wt% Sigma	Atomic %
B	K series	0.20	0.47	0.00081	10.37	5.69	23.96
O	K series	1.38	0.80	0.00465	42.26	3.15	65.96
Zn	L series	0.00	0.39	0.00004	0.25	0.45	0.09
Sr	L series	0.57	0.85	0.00503	16.28	1.47	4.64
Y	L series	0.17	0.79	0.00167	5.14	1.45	1.44
Te	L series	0.40	0.90	0.00307	10.67	1.13	2.09
Dy	L series	0.02	0.71	0.00022	0.74	2.41	0.11
Bi	M series	0.38	0.64	0.00376	14.28	1.49	1.71
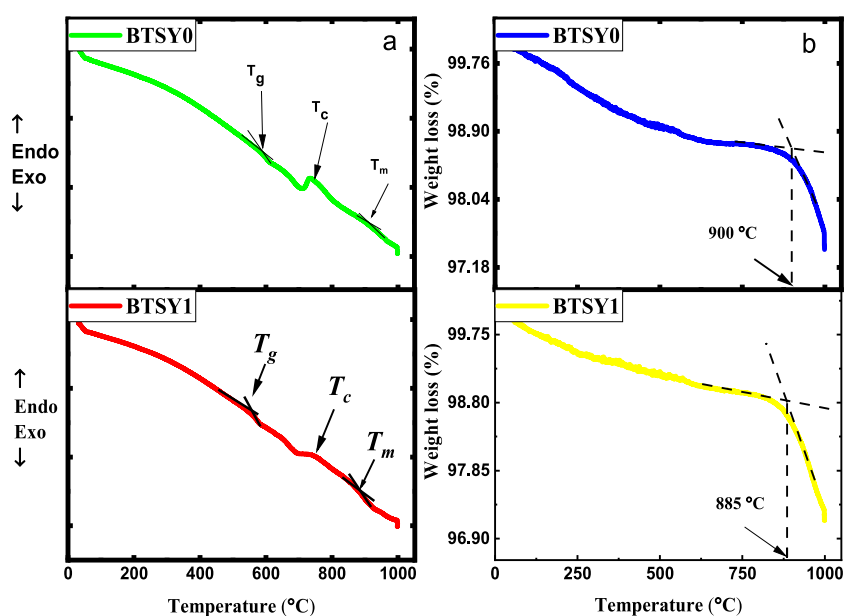
Fig. 6. a) Differential thermal and (b) thermogravimetric curves of the prepared BTSY0 and BTSY1 glass samples.

Table 3
Thermal parameters of prepared samples BTSY0 and BTSY1.

Sample label	T_g (°C) ± 2	T_C (°C) ± 2	T_m (°C) ± 2	$\Delta T = T_c - T_g$ (°C) ± 4	$(T_c - T_g)/T_g$	T_g/T_m	Weight loss (%)
BTSY0	556	735	881	179	0.32	0.63	2.850
BTSY1	589	735	915	164	0.28	0.64	2.593

Table 4
Packing density (Vt), mean atomic volume ($\overline{V}$), (Vt/ $\overline{V}$) ratio and Average bond strength B_{M-O}.

Glass label	Packing density (Vt)	Mean atomic volume ($\overline{V}$)	(V$_t$/ $\overline{V}$) ratio	Average bond strength B_{M-O} (kJ/mol)
BTSY0	0.627	7.070	0.088	205
BTSY1	0.676	6.540	0.103	208

calculated according to the following Equation (6) [48]:

$$B_{A-O} = \frac{G_i}{CN} \tag{6}$$

where *CN* represents the coordination number of the cations, and G_i is the dissociation energy of each oxide. The average single bond strength ($B_{M\text{-}O}$) was obtained by the following relation suggested by Dimitrov and Komatsu Equation (7) [48]:

$$B_{M-O} = \sum x_i (B_{A-O})_i \tag{7}$$

Here x_i represents the molar fraction of each oxide. The values of B_{A-O} for each oxide are listed in Table 4. Based on B_{A-O} values, it can be concluded that the bond of Y–O is stronger than Sr–O, so the average B_{A-O} increased from 205 to 208 for BTSY0 and BTSY1, respectively. The relation between B_{M-O} and T_g is shown in Tables 2 and 3. In Table 5, we list the field strength of cations within the glass matrix. This field strength can reflect how different elements of the glass matrix are stronger and more tightly bound. Field strength values for many cations in the glass system sort in the following order: $Zn^{2+} < Y^{3+} < Dy^{3+} < Sr^{2+} < Bi^{3+}$. Here it can be noted that the field strength for Y^{3+} (1.76) and 1.44 for SrO. Sr^{2+} was replaced by Y^{3+} in the glass system, leading to tighter and stiffer glass samples that supported the V_t and B_{M-O} results.

3.5. Photoluminescence analysis

Fig. 7, illustrates the photoluminescence (PL) emission spectra of the synthesized glass samples. At an excitation of 350 nm (Dy^{3+} excitation), the PL emission occurs due to excitation and de-excitation processes. This excitation causes the Dy ions to be elevated to higher excited states, and the subsequent de-excitation generates the PL emission. The PL spectra showed a broad peak at 550 nm for both s6 and s7 glasses. Additional weak emission peaks were also obtained at 573 and 664 nm, respectively. While the observed broader peak can be linked to the convolution of Bi^{3+} ions transitions corresponding to the non-centrosymmetric site respectively [49], the weak emission bands are due to $^4F_{9/2} \rightarrow \, ^6H_{13/2}$ and $^4F_{9/2} \rightarrow \, ^6H_{11/2}$ Dy^{3+} transitions [50]. Hence, the low symmetrical features of both Bi^{3+} and Dy^{3+} ions were confirmed. The observed Dy^{3+} emission bands agreed with the reports available in the literature [51]. Furthermore, it is worth noting that Y_2O_3 does not undergo radiative transition. Hence all the observed PL emission peaks are either due to the Bi^+ ions or Dy^+ ions present in the glass sample. The $^3P_1 \rightarrow \, ^1S_0$ transition peak appearing in Fig. 7 of the manuscript belongs to Bi^{3+}, not Y_2O_3 [52]. The possibility of energy transfer in the current glass system is from Bi^{3+} to Dy^{3+} as reported in the case of Y_2O_3: Bi, Eu Phosphor, wherein energy transfer from Bi^{3+} to Eu^{3+} was established [52]. However, since there's no change in the intensity of the emission peaks of both Bi^{3+} and Dy^{3+} herein, the possibility of energy transfer was ruled out; a similar situation was adopted by Prakash et al. regarding Bi^{3+} enclosed B_2O_3–SrO–Al_2O_3–PbO glass system doped with Dy^{3+} [53]. The choice of 350 nm excitation energy is due to the fact that it is the strongest band in the absorption edge of the UV–Vis–NIR absorption spectra. Moreover, as the peak shapes remained the same irrespective of the dopants concentration, the broader peak center was red-shifted by about 37 nm. The shifting of the peak center may be linked to the structural re-adjustments induced by the change in the dopants concentration. Again, the constant peak shape indicates that changing the dysprosium ions concentration does not favor structural re-adjustment capable of altering the emission shapes. However, the co-doping effect increased the luminescence intensity of the $^4F_{9/2} \rightarrow \, ^6H_{11/2}$ emission transition. Additionally, the co-doping was found to red-shift the bismuth Bi^{3+} $^3P_1 \rightarrow \, ^1S_0$ transition but with constant intensity. The observed trend stressed the ability of rare earth ions co-doping technique to enhance the luminescence and, thus, the optical properties of the developed glass systems [54]. According to the literature, the enhancement is due to energy transfer between the rare earth ions when the critical distance between them is attained. In the present case, the energy transfer is from Y^{3+} to Dy^{3+} and was probably mediated by electric dipole-dipole mechanism. Hence, the large super-broadband emission was achieved, and the carrier mobility increased [55].

3.6. Mechanical properties

Glass' mechanical properties are influenced by various kinds of factors, the most important of which are the microstructure and the arrangement of crystalline phases. These characteristics play an important role in defining glass's mechanical behaviour, strength, and durability [56]. The microstructure of a glass matrix is the arrangement and distribution of atoms, molecules, and flaws that influence its overall strength and structural integrity [57,58]. Furthermore, the crystalline assembly, or the presence or absence of crystalline areas inside the glass, influences qualities such as hardness, cracking, and deformation resistance [59]. The hardness of glass materials is usually referred to as resistance to abrasion and scratching [56]. The microhardness test can measure the strength glassy, in this regard, indentation hardness is a useful method for examining the mechanical characteristics of small-volume materials, in which a fixed stress on the diamond indenter is applied and measured using a microscope [60]. Vickers hardness is the most often used geometric indenter in hardness testing. The ratio of applied load to contact surface (area) is the diamond pyramid hardness number HV [61]. Low load hardness tests were conducted with load levels of 40 N with a dwell period of 10s per the method [40,62]. Table 6 lists the hardness values for BTSY0 and BTSY1 glass samples. Adding Y_2O_3 instead of SrO enhanced the hardness from 536.7 to 1366.9 as shown in Fig. 8. The obtained results are in line with the previous results.

Table 5
Coordination number, electronegativity, single bond strength and field strength values.

Metal ion	CN	Z	Electronegativity	Single bond strength B_{A-O} (kJ/mol)	Ionic radius ($\overset{o}{A}$)	Field strength ($\overset{o}{A}{}^{-2}$)
Te^{6+}	6	6	2.10	63	—	—
B^{3+}	3	3	2	270	—	—
Sr^{2+}	8	2	1	53	1.13	1.44
Bi^{3+}	8	3	1.9	56	1.17	1.40
Zn^{2+}	6	2	1.6	63	0.74	2.21
Dy^{3+}	8	3	1.4	77	1.05	1.56
Y^{3+}	6	3	1.2	89	0.93	1.76
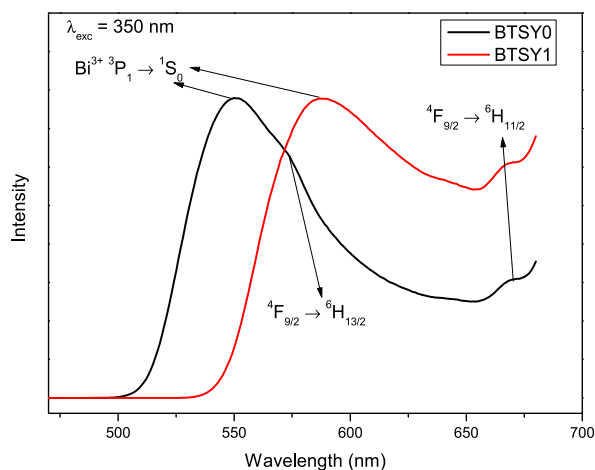
Fig. 7. Photoluminescence spectra of BTSY0 and BTSY1 glasses.

Table 6
Vickers hardness of the synthesized glasses system BTSY0 and BTSY1.

Glass sample	Hardness	D1±005	D2±0011	HV(Gpa) ±09
BTSY0	536.7 ± 18	0.0588	0.0587	1.262
BTSY1	1366.9 ± 33	0.0357	0.0380	1.950
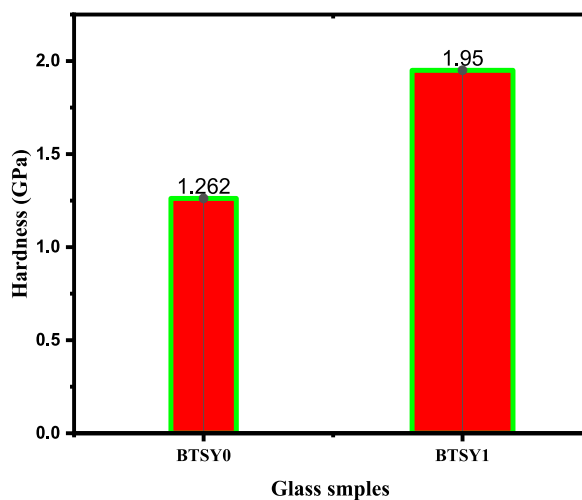
Fig. 8. Show the hardness of the glass samples.

4. Conclusion

The melt-quenching process successfully prepared a tellu-borate glass matrix with a new composition. We investigated the glasses' excellent physical, structural, chemical, thermal, and optical properties. It was revealed that adding Y_2O_3 into the glass matrix could enhance these properties, including the mechanical properties. The correlation between the structural and thermal properties was confirmed. These changes were based on the generation of non-bridging oxygen in the glass network, thereby altering the associated packing density as well as the Vickers hardness. The revealed optical properties indicate the suitability of the glasses for a wide range of scientific and technological applications. The limitations of the study lie in the inadequate sample size for drawing valid conclusions. However, the disclosed results still provide insight into the applicability of the designed glass systems in various scientific arenas.

Author contribution statement

Hammam Abdurabu Thabit: Conceived and designed the experiments, Performed the experiments, Wrote the paper.

M.H.A. Mhareb; DA Abdulmalik; Y.S.M. Alajerami: Analyzed and interpreted the data, Wrote the paper.

Abdullahi, I: Performed the experiments, Wrote the paper.

Mohammed Al-Fakih: Conceived and designed the experiments; S.Hashim; Abd Khamim Ismail: Contributed reagents, materials, analysis tools.

Data availability statement

Data included in article/supp. material/referenced in article.

Declaration of competing interest

The authors declare that they have no known competing financial interests or personal relationships that could have appeared to influence the work reported in this paper.

Acknowledgments

Appendix A. Supplementary data

Supplementary data to this article can be found online at https://doi.org/10.1016/j.heliyon.2023.e18309.

References

[1] H.A. Thabit, et al., Preparation, characterization, and mechanical-optical properties of telluro-borate glasses containing tungsten, Ceram. Int. 49 (16) (2023) 26505–26515.

[2] R.L. Sutherland, Handbook of Nonlinear Optics, CRC press, 2003.

[3] B. Shanmugavelu, et al., Third order nonlinear optical properties of bismuth zinc borate glasses, J. Appl. Phys. 114 (24) (2013), 243103.

[4] K.A. Bashar, et al., Tunable white-light emission from Pr3+/Dy3+ co-doped B2O3 - TeO2 PbO - ZnO Li2O - Na2O glasses, Opt. Mater. 88 (2019) 558–569.

[5] M.H.A. Mhareb, et al., Physical and optical properties of Li2O-MgO-B2O3 doped with Dy3+, Opt Spectrosc. 117 (4) (2014) 552–559.

[6] H.A. Thabit, et al., Physical, optical and spectroscopic characteristics investigation for doped Dy3+ borate glass matrix, J. Non-Cryst. Solids 608 (2023), 122258.

[7] S. El-Kameesy, H. Thabit, Radionuclides concentrations in some rock samples used as building material from Yafea area in Yemen, Arab J. Nuc. Sci. App. 49 (1) (2016) 46–52.

[8] L. Shamshad, et al., Luminescence characterization of Sm3+-doped sodium potassium borate glasses for laser application, J. Alloys Compd. 766 (2018) 828–840.

[9] Y.S. Rammah, et al., Optical properties of bismuth borotellurite glasses doped with NdCl3, J. Mol. Struct. 1175 (2019) 504–511.

[10] A.H. Hammad, A.M. Abdelghany, Optical and structural investigations of zinc phosphate glasses containing vanadium ions, J. Non-Cryst. Solids 433 (2016) 14–19.

[11] S.A. Reduan, et al., Physical and optical properties of Li2O–MgO–B2O3 doped with Sm3+, J. Mol. Struct. 1060 (2014) 6–10.

[12] S. Tanabe, Rare-earth-doped glasses for fiber amplifiers in broadband telecommunication, Compt. Rendus Chem. 5 (12) (2002) 815–824.

[13] S. Hashim, et al., Luminescence features of dysprosium and phosphorus oxide co-doped lithium magnesium borate glass, Radiat. Phys. Chem. 137 (2017) 45–48.

[14] O. Madkhali, et al., Structural and temperature dependence luminescence characteristics of RE (RE=Eu3+, Dy3+, Sm3+ and Tb3+) in the new gadolinium aluminate borate phosphor, Ceram. Int. 49 (12) (2023) 19982–19995.

[15] K.N. Kumar, et al., Non-cytotoxic Dy3+ activated La10W22O81 nanophosphors for UV based cool white LEDs and anticancer applications, Spectrochim. Acta Mol. Biomol. Spectrosc. 278 (2022), 121309.

[16] M. Zekri, et al., Experimental and theoretical studies of Dy3+ doped alkaline earth aluminosilicate glasses, J. Lumin. 212 (2019) 354–360.

[17] Sonali, C. Shivakumara, *Enhanced emission intensity in (Li+/Ca2+/Bi3+) ions co-doped NaLa(MoO4)2: Dy3+ phosphors and their Judd-Ofelt analysis for WLEDs applications*, Methods Appl. Fluoresc. 11 (2) (2023) 024001.

[18] K. Li, R. Van Deun, Color tuning from greenish-yellow to orange-red in thermal-stable KBaY (MoO4) 3: Dy3+, Eu3+ phosphors via energy transfer for UV W-LEDs, ACS Appl. Electr. Mater. 2 (6) (2020) 1735–1744.
[19] C. Nandanwar, N. Kokode, Synthesis and photoluminescence properties of Ca5 (PO4) 3F: Ln (Ln: Dy3+, Eu3+ and Sm3+) phosphors for near UV-based solid state lighting, Phys. Chem. Solid State 23 (3) (2022) 597–603.
[20] L.D. Pye, V.D. Fréchette, N.J. Kreidl, Borate Glasses: Structure, Properties, Applications, vol. 12, Springer Science & Business Media, 2012.
[21] Y. Alajerami, et al., Physical, structural, and shielding properties of cadmium bismuth borate-based glasses, J. Appl. Phys. 127 (17) (2020), 175102.
[22] D. Ege, K. Zheng, A.R. Boccaccini, Borate bioactive glasses (BBG): bone regeneration, wound healing applications, and future directions, ACS Appl. Bio Mater. 5 (8) (2022) 3608–3622.
[23] H.A. Thabit, N.A. Kabir, The study of X-ray effect on structural, morphology and optical properties of ZnO nanopowder, Nucl. Instrum. Methods Phys. Res. B Beam Interact. Mater. Atoms 436 (2018) 278–284.
[24] H.A. Thabit, et al., Development of Ag-doped ZnO thin films and thermoluminescence (TLD) characteristics for radiation technology, Nanomaterials 12 (17) (2022) 3068.
[25] H.A. Thabit, et al., Investigation of the thermoluminescence dosimeter characteristics of multilayer ZnO (300 nm)/Ag (50 nm)/ZnO (x) thin films for photonic dosimetry applications, Opt. Mater. 137 (2023), 113548.
[26] R. Zhao, et al., Catalytic nanozyme for radiation protection, Bioconjugate Chem. 32 (3) (2021) 411–429.
[27] Y. Anantha lakshmi, et al., Photoluminescence properties of Sm3+ ions doped Bismuth Boro tellurite glasses, Solid State Sci. 116 (2021), 106609.
[28] V. Rivera, F. Ferri, E. Marega, Tellurite glasses for plasmonics, Technolog. Adv. Tellurite Glasses: Proper. Process. App. (2017) 301–330.
[29] M.H.A. Mhareb, et al., The impact of TeO2 on physical, structural, optical and radiation shielding features for borate glass samples, Optik 247 (2021), 167924.
[30] N. Dwaikat, et al., Durability, optical and radiation shielding properties for new series of boro-tellurite glass, Optik 245 (2021), 167667.
[31] B. Suresh, et al., Influence of Bi3+ ions on the amplification of 1.3μm emission of Pr3+ ions in lead silicate glasses for the applications in second telecom window communications, J. Lumin. 182 (2017) 312–322.
[32] J. Ashok, et al., Studies on dielectric dispersion, relaxation kinetics and a.c. conductivity of Na2OCuOSiO2 glasses mixed with Bi2O3-Influence of redox behavior of copper ions, J. Alloys Compd. 696 (2017) 1260–1268.
[33] L. Gritsch, et al., Bioactive glass-based organic/inorganic hybrids: an analysis of the current trends in polymer design and selection, J. Mater. Chem. B 11 (3) (2023) 519–545.
[34] M. Atef Cherbib, et al., Effect of SrO content on the structure and properties of sodium-strontium metaphosphate glasses, J. Phys. Chem. Solid. 102 (2017) 62–68.
[35] S. Kargozar, et al., Multiple and promising applications of strontium (Sr)-containing bioactive glasses in bone tissue engineering, Front. Bioeng. Biotechnol. 7 (2019) 161.
[36] H.A. Thabit, et al., A closer look at the structure and gamma-ray shielding properties of newly designed boro -tellurite glasses reinforced by bismuth (III) oxide, Nucl. Eng. Technol. 55 (5) (2023) 1734–1741.
[37] E.A. Davis, N.F. Mott, Conduction in non-crystalline systems V. Conductivity, optical absorption and photoconductivity in amorphous semiconductors, Phil. Mag.: J. Theor. Exp. Appl. Phy. 22 (179) (1970) 903–922.
[38] M.I. Sayyed, et al., Structural, optical, and shielding investigations of TeO2–GeO2–ZnO–Li2O–Bi2O3 glass system for radiation protection applications, Appl. Phys. A 125 (2019) 1–8.
[39] K. Chandra Sekhar, et al., The effect of the addition of CaF2 and PbF2 on boro-tellurite glasses doped with chromium ions, Mater. Res. Express 6 (12) (2019), 125206.
[40] H.A. Thabit, et al., Structural, thermal, and mechanical investigation of telluro-borate-Bismuth glass for radiation shielding, J. Mater. Res. Technol. 24 (2023) 4353–4363.
[41] Y.B. Saddeek, M.A. Azooz, A.B. Saddek, Ultrasonic investigations of some bismuth borate glasses doped with Al2O3, Bull. Mater. Sci. 38 (1) (2015) 241–246.
[42] A. Dietzel, Glass structure and glass properties, Glass 22 (1968) 41.
[43] H.A. Saudy, et al., Mechanical, Thermal and Chemical Durability Behaviors of CdO-Bi 2 O 3 Boro-Phosphate Glasses Containing Fe 2 O 3, 2013.
[44] G.M. Asnag, A.H. Oraby, A.M. Abdelghany, Green synthesis of gold nanoparticles and its effect on the optical, thermal and electrical properties of carboxymethyl cellulose, Compos. B Eng. 172 (2019) 436–446.
[45] S. Bhatti, S. Santokh, Ultrasonic Studies in some barium borate glasses, J. Pure Appl. Ultrason. 8 (1986) 101.
[46] K. Zhao, et al., Correlation between atomic size and elastic properties/glass transition temperature in metallic glasses, Sci. China Phys. Mech. Astron. 60 (2017), 106121.
[47] A.A. El-Moneim, H.Y. Alfifi, A new factor for predicting the acoustical properties of oxide glasses, Eur. J. Glasses Sci. Technol. B Phys. Chem. Glasses 59 (2) (2018) 97–105.
[48] K.H. Sun, Fundamental condition of glass formation, J. Am. Ceram. Soc. 30 (9) (1947) 277–281.
[49] A. Scarangella, et al., Visible emission from bismuth-doped yttrium oxide thin films for lighting and display applications, Sci. Rep. 7 (1) (2017), 17325.
[50] I. Abdullahi, et al., Structures and spectroscopic characteristics of barium-sulfur-telluro-borate glasses: role of Sm3+ and Dy3+ Co-activation, Mater. Chem. Phys. 247 (2020), 122862.
[51] Y. Dai, et al., Single-composition white light emission from Dy(3+) doped Sr₂CaWO₆, Materials 12 (3) (2019).
[52] G. Ju, et al., White-light generation and energy transfer in Y2O3:Bi,Eu phosphor for ultraviolet light-emitting diodes, J. Electrochem. Soc. 158 (10) (2011) J294.
[53] A.H.D. Prakash, et al., Synthesis and characterization of B2O3–Bi2O3–SrO–Al2O3–PbO–Dy2O3 glass system: the role of Bi2O3/Dy2O3 on the optical, structural, and radiation absorption parameters, Mater. Res. Bull. 155 (2022), 111952.
[54] M.M. Martins, et al., Tm3+ doped Bi2O3-GeO2 glasses with silver nanoparticles for optical amplifiers in the short-wave-infrared-region, J. Alloys Compd. 772 (2019) 58–63.
[55] J. Zhang, et al., A brief review of co-doping, Front. Phys. 11 (2016) 1–21.
[56] A. Al-Amri, J. Evans, Degradation of the strength of glass after light contact with other materials, Mater. Sci. Eng., A 177 (1–2) (1994) 11–18.
[57] I. Abdullahi, et al., Enhanced up- and down-conversion luminescence from Dy3+-Sm3+ co-doped B2O3-SrCO3-TeO2-Al2O3-MgO glass hosts: effects of CuO nanoparticles embedment, Phys. Scripta 98 (6) (2023), 065511.
[58] S.A. Jupri, et al., Spectroscopic traits of holmium in magnesium zinc sulfophosphate glass host: judd – Ofelt evaluation, J. Alloys Compd. 753 (2018) 446–456.
[59] Y. Yang, et al., Effect of Ag substitution for Ti on glass-forming ability, thermal stability and mechanical properties of Zr-based bulk metallic glasses, Mater. Sci. Eng., A 746 (2019) 229–238.
[60] R. Laopaiboon, C. Bootjomchai, Characterization of elastic and structural properties of alkali-borosilicate glasses doped with vanadium oxide using ultrasonic technique, Glass Phys. Chem. 41 (4) (2015) 352–358.
[61] S. Sawamura, L. Wondraczek, Scratch hardness of glass, Phys. Rev. Mater. 2 (9) (2018), 092601.
[62] S.Y. Marzouk, Ultrasonic and infrared measurements of copper-doped sodium phosphate glasses, Mater. Chem. Phys. 114 (1) (2009) 188–193.